ARTICLE

OBC
www.rsc.org/obc

Neighbouring group processes in the deamination of protonated phenylalanine derivatives†‡

Hadi Lioe[a,b] and Richard A. J. O'Hair*[a,b]

[a] *School of Chemistry, University of Melbourne, Victoria, 3010, Australia*
[b] *Bio21 Institute, The University of Melbourne, Victoria, 3010, Australia.*
E-mail: rohair@unimelb.edu.au; Fax: +61 3 9347-5180; Tel: +61 3 8344-2452

Received 7th March 2005, Accepted 22nd August 2005
First published as an Advance Article on the web 15th September 2005

The gas-phase fragmentation of protonated phenylalanine and a series of its derivatives (tyrosine, 4-methylphenylalanine, 4-aminophenylalanine, 4-methoxyphenylalanine, 4-*tert*-butylphenylalanine, 4-fluorophenylalanine, 4-chlorophenylalanine, 4-bromophenylalanine, 4-iodophenylalanine, 4-cyanophenylalanine, 4-nitrophenylalanine, 3-fluorophenylalanine, and 3,4-dichlorophenylalanine) were examined using a combination of low energy CID in a quadrupole ion trap mass spectrometer as well as DFT calculations and RRKM modelling. In particular, the relationship between the electron-donating ability of the substituent and the competitive losses of H_2O + CO and NH_3 were explored through the application of the Hammett equation. It was found that electron-donating substituents promote the loss of NH_3, while electron-withdrawing substituents suppress the loss of NH_3 and favour the H_2O + CO loss fragmentation channel instead. These observations are consistent with a neighbouring group pathway operating for the loss of NH_3. Molecular orbital calculation (at the B3LYP/6-31+G(d,p) level of theory) were also performed for a range of derivatives to compare the relative transition state energy barriers for three competing mechanisms: (i) the combined loss of H_2O + CO, which is triggered by an initial intramolecular proton transfer from the ammonium group to hydroxyl OH, followed by the combined loss of H_2O and CO to form an immonium ion; (ii) loss of NH_3 *via* an aryl assisted neighbouring group pathway to yield a phenonium ion; (iii) loss of NH_3 *via* a 1,2-hydride migration process, which results in the formation of a benzyl cation. The relative energy barriers for H_2O + CO loss remain nearly constant, while that for both NH_3 pathways increase as the substituent moves from electron-donating to electron-withdrawing. The relative transition state energy for loss of NH_3 *via* the aryl assisted neighbouring group pathway is always lower than that of the 1,2-hydride migration process. RRKM modelling of the DFT predicted barrier heights suggest that the rate constants for H_2O + CO loss are insensitive to the substituent on the ring, while the NH_3 loss channels are greatly affected by the substituent. These theoretical results are consistent with the experimental observation of the relative yields of the competing fragmentation channels. Finally, comparisons with published gas phase and condensed phase studies on related systems are made.

Introduction

Significant efforts have been directed at understanding the gas phase fragmentation reactions of peptide ions to facilitate the use of tandem mass spectrometry (MS/MS) in proteomics applications.[1] Two main approaches have been adopted: (i) examination of mechanisms of model systems ranging from amino acids to small peptides using "physical organic" tools and concepts;[2] (ii) interrogation and statistical analyses of databases of thousands of MS/MS spectra of "real world" peptides derived from tryptic digests to evaluate preferred sites of cleavage.[3] One of the most important conclusions from such studies is that many of the fragmentation reactions of protonated peptides which occur under low energy collision induced dissociation (CID) conditions involve neighbouring group pathways, whereby a nearby nucleophile attacks an electrophilic centre to facilitate bond cleavage.[4] We have previously classified these reactions as: backbone–backbone; side chain–backbone and backbone–side chain, depending on whether the nucleophile and electrophile are on either the backbone or side chain.[2] Of particular interest is that a number of gas phase neighbouring group pathways have been discovered which have direct solution phase analogies. For example nucleophilic attack of amino acid side chains can facilitate the deamination of protonated amino acids and their derivatives. Thus the sulfhydryl group of cysteine facilitates loss of NH_3 to form an episulfonium ion (eqn 1),[5] in direct analogy to the formation of thiiranecarboxylic acids when cysteine is treated with sodium nitrite and hydrochloric acid in the condensed phase (eqn 2).[6] More recently we have shown that the side chain of tryptophan also facilitates the loss of NH_3 *via* the formation of a spirocyclopropane intermediate (eqn 3),[7] which also has analogies in the reaction of related indoles (eqn 4).[8]

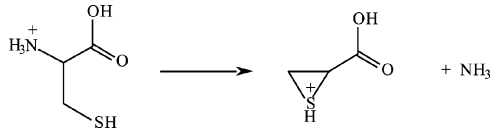

(1)

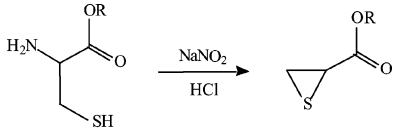

(R = H, CH_3)

(2)

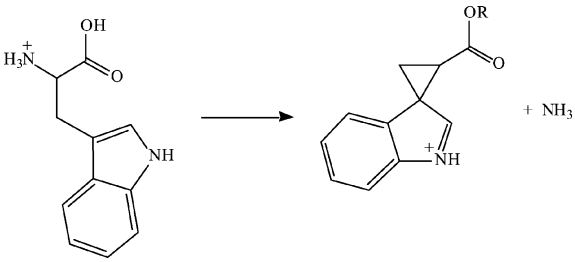

(3)

† Electronic supplementary information (ESI) available: Hammett plots, optimized structures and energy data. See http://dx.doi.org/10.1039/b503355a

‡ This paper is Part 45 of the series "Gas-phase ion chemistry of biomolecules".[50]

DOI:10.1039/b503355a

 This journal is © The Royal Society of Chemistry 2005

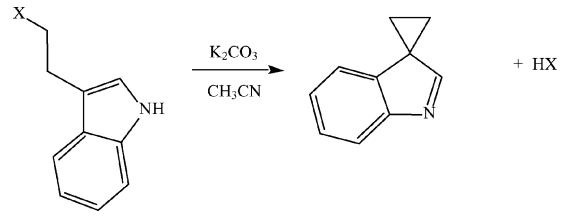

(4)

Despite the success in cataloguing the types of fragmentation reactions available for protonated peptides and amino acids, no computer program has yet been developed which can accurately predict both the types of fragment ions formed as well as their relative abundances. The basis for a predictive model of peptide ion fragmentation would require a description of the intrinsic properties of an individual peptide, such as the type and nature of amino acid residues present, site of protonation, presence of post-translational modification, *etc.*, and how the combination of these properties affects the mechanisms of the fragmentation of the peptide ions. The progress made in determining the mechanisms of peptide fragmentation reactions has been recently reviewed.[9]

Linear free energy correlations are one of the most powerful physical organic chemistry tools which have provided useful mechanistic insight into numerous solution phase and gas phase reactions.[10–13] While they have been used to rationalize gas phase fragmentation[12] and to predict the appearance of mass spectra,[10,14–16] their applications to facilitate an understanding of the gas phase fragmentation reactions of amino acid and peptide ions are limited.[16–18] Examples include the work of Morgan and Bursey[17,18] and Harrison[19,20] who used linear free energy correlations to relate the relative abundances of sequence ions for amide bond cleavage reactions in simple protonated di- and tripeptides. Given that previous reports have demonstrated a substituent effect for deamination of protonated phenylalanine derivatives (tyrosine yields greater loss of NH_3 than phenylalanine[21–25]), in this work we have undertaken a detailed study of the gas-phase fragmentation of a series of protonated phenylalanine derivatives **A**, where: R_4 = NO_2, CN, I, Br, Cl, F, H, Me, ^{t}Bu, OH, OMe, NH_2; R_3 = F; R_3 = R_4 = Cl using low energy CID in a quadrupole ion trap mass spectrometer. The relationship between the electron-donating ability of the substituent and the competitive losses of H_2O + CO and NH_3 (Scheme 1) are explored through the application of the Hammett equation. Molecular orbital calculations were also performed to establish whether a neighbouring group mechanism operates to form **C** and to estimate the transition state energy barriers for competing mechanisms for a range of derivatives (R_4 = NH_2, OH, Me, H, Cl, NO_2). Additionally, the variations in the unimolecular rate constant for the competitive losses of H_2O + CO and NH_3 for different substituents were determined using RRKM modelling. Finally, comparisons with published condensed phase studies on related systems are made.[26,27]

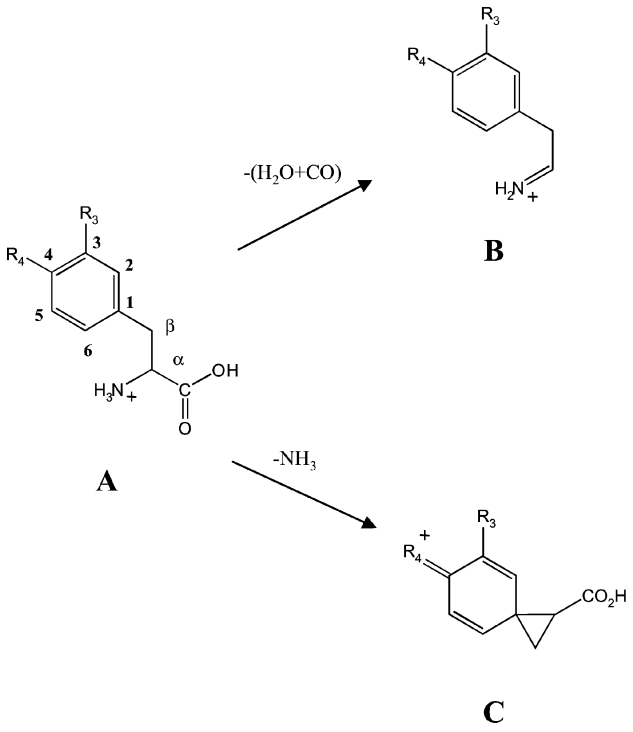

R_4 = NO_2, CN, I, Br, Cl, F, H, Me, ^{t}Bu, OH, OMe, NH_2
R_3 = F
R_3 = R_4 = Cl

Scheme 1

Experimental

Materials

Phenylalanine was purchased from Sigma Chemical Co. (St. Louis, MO). Tyrosine and 4-methylphenylalanine (4-Me Phe) were purchased from BACHEM (Bubendorf, Switzerland). 4-Aminophenylalanine (4-NH_2 Phe), 4-methoxyphenylalanine (4-OMe Phe), 4-*tert*-butylphenylalanine (4-^{t}Bu Phe), 4-fluorophenylalanine (4-F Phe), 4-chlorophenylalanine (4-Cl Phe), 4-bromophenylalanine (4-Br Phe), 4-iodophenylalanine (4-I Phe), 4-cyanophenylalanine (4-CN Phe), 4-nitrophenylalanine (4-NO_2 Phe), 3-fluorophenylalanine (3-F Phe), and 3,4-dichlorophenylalanine (3,4-Cl_2 Phe) were purchased from Peptech Corporation (Burlington, MA). Methanol (ChromAR grade) was purchased from Mallinkrodt (Melbourne, Australia). Acetic acid was obtained from Merck (Darmstadt, Germany). Triply distilled (Milli-Q®) water was used for all sample preparation and analysis by mass spectrometry.

Mass spectrometry

Protonated phenylalanine derivatives were formed *via* electrospray ionization (ESI) on a Finnigan model LCQ (San Jose, CA, USA) quadrupole ion trap mass spectrometer. Sample mixtures in 50% CH_3OH–50% H_2O containing 0.1 M acetic acid (total concentration is 2 mM) were introduced to the mass spectrometer at 5 μL min^{-1}. The spray voltage was set at 4.5 kV. Nitrogen sheath gas was supplied at 25 psi. The heated capillary temperature was 200 °C. The signal for the $[M + H]^+$ ion of the amino acids was maximized by tuning the capillary and tube lens voltages, which typically were in the range of: capillary voltage 0 to 20 V and tube lens −5 to −10 V. The $[M + H]^+$ ions were selected with a window of 2.5 Th and were subjected to CID with a Q value of 0.25 and activation time of 30 ms. The activation amplitude was adjusted to allow 50% of precursor ion to remain (this corresponds to activation amplitude ranging from 0.45 to 0.57 V). All experiments were performed three times for proper statistical analysis, with an average of 30 scans for each run.

Construction of the Hammett plot

For each experiment, the relative abundance of each peak was calculated by integrating the peak area. The Z-values for all derivatives are calculated for each small molecule loss (NH_3 and H_2O + CO loss), where Z = (ion abundance for NH_3 loss or H_2O + CO loss)/(sum of all ion abundances). The Z-values therefore represent the normalized ion intensity so that they can be directly compared to the other substituents. By assuming that $\log \frac{k_x}{k_h} \approx \log \frac{Z}{Z_0}$, where Z_0 is the corresponding Z-value for phenylalanine (R_4 = H), the Hammett plots are then

constructed by plotting $\log(Z/Z_0)$ against the Brown–Okamoto substituent constant (σ_X^+).[28] The sign of the substituent constant is such that $\sigma < 0$ indicates a more electron-donating group relative to hydrogen and conversely, $\sigma > 0$ indicates a more electron-withdrawing group relative to hydrogen. All values of the substituent constants were adopted from a comprehensive review by Hansch *et al.*[29] The reaction constant (ρ) was evaluated from the slope of the linear regression of the Hammett plot. A positive value of the reaction constant represents reactions that are enhanced by the presence of electron-withdrawing substituent, and *vice versa*. All errors are stated at the 95% confidence limit.

Computational methods

All structure optimization was performed using Gaussian 03[30] molecular modelling package on a Dell PowerEdge 400SC Server available from the Melbourne Advanced Research Computing Centre or a Pentium 4 computer. Structures of minima and transition states were optimized at the B3LYP level of theory with the standard 6-31+G(d,p) basis set.[31] All transition state structures were found using the normal Gaussian keyword for transition state optimization, except for NH_3 loss *via* pathway 2 of Scheme 2 for the systems Phe and 4-NO_2 Phe, which were eventually located with the additional "CalcAll" keyword. The exit channel in the acylium–H_2O ion–molecule complex for the H_2O + CO loss channel was located by stretching the C–CO bond to *ca.* 2.0 Å, and then optimized for a transition state to find the second transition state (**TS1b**). All optimized structures were subjected to vibrational frequency analysis and visualized using the computer package GaussView 2.1[30] to determine the nature of the stationary points. Intrinsic reaction coordinate (IRC) runs were performed on each transition state, followed by geometry optimizations to check that they connected to the appropriate reactant and product ion minima. The final energies used to calculate the potential energy surfaces involve correcting the electronic energies with the unscaled zero-point vibrational energies.

Calculation of unimolecular rate constant using RRKM approach

The rate constants of the competing pathways were approximated using Rice–Ramsperger–Kassel–Marcus (RRKM) calculation using DFT calculated data. The RRKM rate constant expression is given by eqn 5:

$$k(E) = \frac{\sigma W^{\ddagger}(E - E_0)}{h\rho(E)} \quad (5)$$

where σ is the reaction degeneracy, E_0 is the critical energy of activation, $W^{\ddagger}(E–E_0)$ is the sum of vibrational states of the transition states from energy 0 to $E–E_0$, $\rho(E)$ is the density of vibrational states of the reactants at energy E, and h is Planck's constant. The sum and density of vibrational states were evaluated using the semiclassical Whitten–Rabinovitch approximation[32] which is known to produce very accurate approximations for small systems with reduced energy >0.1 eV.[32–34] We used a modified RRKM program compiled originally by Laskin and Futrell in Microsoft Excel as part of RRKM modelling of fragmentation efficiency curves.[35–37] The E_0 and vibrational frequencies of reactant and transition state were obtained from DFT calculation at B3LYP/6-31+G(d,p) level of theory. No scaling factor is used for the E_0 and vibrational frequencies. The RRKM rate constants for the competing fragmentation pathways were determined using the energy range from E_0 to 100 kcal mol^{-1}. Complete structural details and electronic energy and zero point vibrational energy for each B3LYP/6-31+G(d,p) optimized structure are available in the supplementary material.

Results and discussion

(1) MS/MS and linear free energy correlation in the fragmentation of protonated *para*-substituted phenylalanine derivatives

The MS/MS of selected protonated *para*-substituted Phe are shown in Fig. 1 as a function of electron-donating ability, while Table 1 summarizes the MS/MS of all 14 protonated Phe derivatives studied, listed according to increasing Brown–Okamoto substituent constants (σ^+). Protonated Phe mainly fragments under quadrupole ion trap CID conditions, *via* the loss of H_2O + CO, although a minor loss of NH_3 is also observed (Fig. 1c). In contrast, protonated Tyr shows an enhanced loss of NH_3 relative to the H_2O + CO channel (Fig. 1b). These findings are consistent with previous studies,[21,23,38] with NH_3 loss from protonated tyrosine being observed under a range

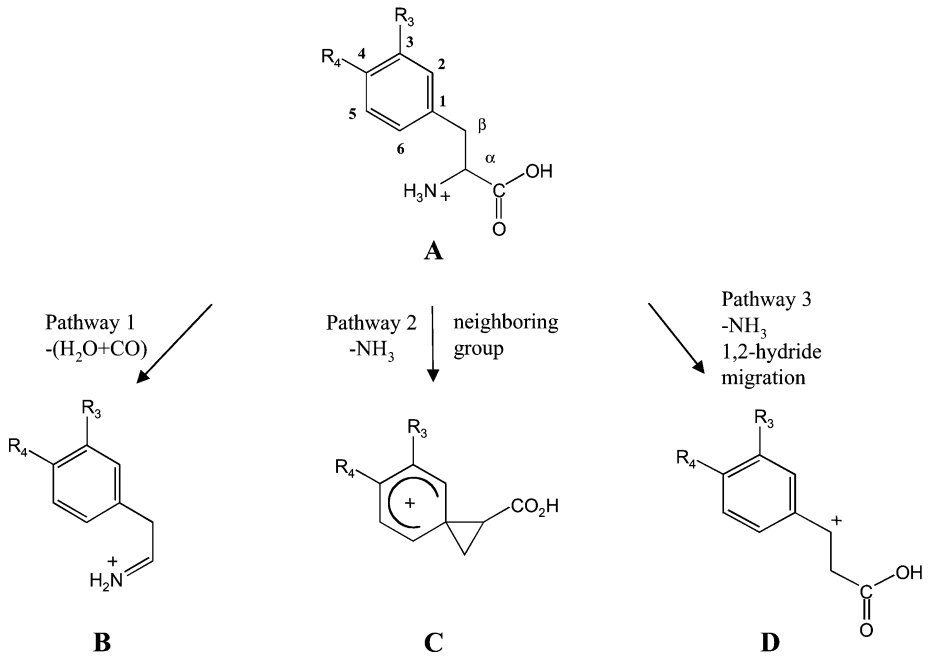

Scheme 2

Table 1 Summary of the CID MS/MS data of all protonated substituted phenylalanine studied

Substituted Phe[a]	$[M + H]^+$	Product ion: m/z, (loss), abundance (%)	σ_x^+ [b]
$R_4 = NH_2$	181	181, (NH_3), 100	−1.3
$R_4 = OH$	182	165, (NH_3), 100; 136, (H_2O + CO), 22	−0.92
$R_4 = OMe$	196	179, (NH_3), 100; 150, (H_2O + CO), 7	−0.78
$R_4 = Me$	180	163, (NH_3), 81; 134, (H_2O + CO), 100	−0.31
$R_4 = {}^tBu$	222	205, (NH_3), 100; 176, (H_2O + CO), 80; 166, ($CH_2{=}(CH_3)_2$), 8; 149, (NH_3 + $CH_2{=}(CH_3)_2$), 21	−0.26
$R_4 = F$	184	167, (NH_3), 17; 138, (H_2O + CO), 100	−0.07
$R_4 = H$	166	149, (NH_3), 6; 120, (H_2O + CO), 100	0.0
$R_4 = Cl$	200	183, (NH_3), 14; 154, (H_2O + CO), 100	0.11
$R_4 = I$	292	275, (NH_3), 28; 246, (H_2O + CO), 100	0.14
$R_4 = Br$	244	227, (NH_3), 18; 198, (H_2O + CO), 100	0.15
$R_3 = F$	184	138, (H_2O + CO), 100	0.34
$R_3 = R_4 = Cl$	234	217, (NH_3), 3; 188, (H_2O + CO), 100	0.48
$R_4 = CN$	191	145, (H_2O + CO), 100	0.66
$R_4 = NO_2$	211	165, (H_2O + CO), 100	0.79

[a] Listed according to increasing electron-withdrawing capability (more positive σ^+). See Scheme 1 for structures. [b] The substituent constant values were adapted from ref. 29.

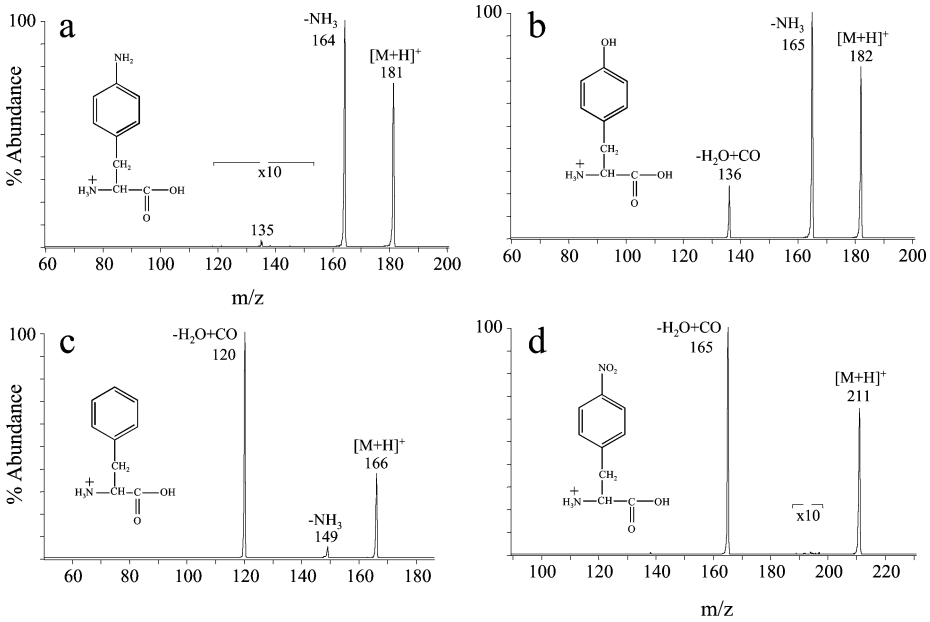

Fig. 1 CID MS/MS spectra of selected $[M + H]^+$ ion of protonated *para*-substituted phenylalanine derivatives: (a) 4-NH_2 Phe, (b) 4-OH Phe, (c) Phe, and (d) 4-NO_2 Phe.

of conditions.[39] The competing NH_3 loss pathway has been rationalized to occur *via* intramolecular attack of the electron rich aryl ring onto the alpha carbon to form the phenonium ion **C**[22] (a side chain–backbone mechanism[2]). Further examination of Fig. 1 and Table 1 clearly illustrates how ring substituents can dramatically alter the relative ratios of the competing NH_3 and H_2O + CO loss fragmentation channels for phenylalanine derivatives. It is clearly evident that as σ^+ becomes more negative (the substituent becomes more electron-donating), the percentage of NH_3 loss increases, and while at the same time the percentage of H_2O + CO loss decreases. The extreme examples are the 4-NH_2 Phe derivative, with its powerful electron-donating group solely directing NH_3 loss (Fig. 1a) and the electron deficient aryl ring of 4-NO_2 Phe, which is a such poor neighbouring group that it only fragments *via* the combined loss of H_2O + CO (Fig. 1d).

In order to address whether it is possible to quantify the role of electron-donating groups in promoting NH_3 loss, we have used the raw ion abundances for all ions present in the MS/MS spectra (see the Experimental section for a more detailed discussion) to construct Hammett plots for the competing fragmentation pathways from the protonated phenylalanine derivatives, and these are shown in Fig. 2. Both plots were constructed using the Brown–Okamoto substituent constant, which is known to account for the effects of through-conjugation. Interaction

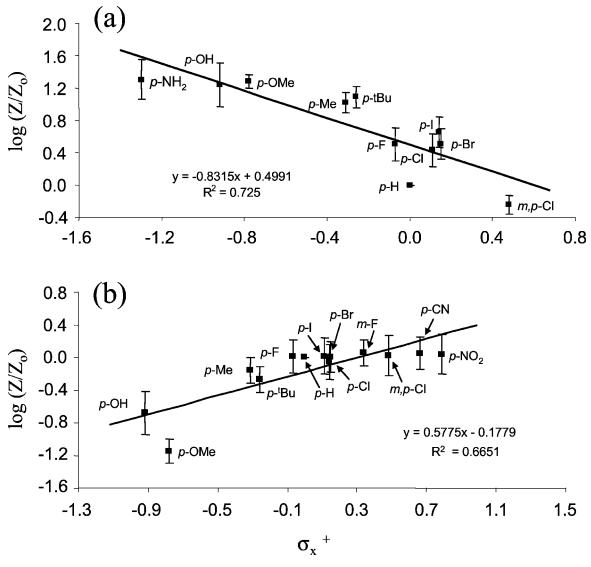

Fig. 2 The Hammett plot for (a) NH_3 loss and (b) H_2O + CO loss from all protonated substituted phenylalanine derivatives studied constructed using Brown–Okamoto substituent constant (σ_x^+). Error bars represent 95% confidence intervals.

of the substituent with the reaction centre (backbone) of the molecule through space would be negligible for *para*-substituted phenylalanine derivatives due to the rigidity of the planar aromatic ring, and at the same time through-bond interaction would be minimal since the substituent is remote to the reaction center. Hence through-conjugation is the dominant interaction between the substituent and the reaction centre. Note that NH_3 loss is not observed in the CID MS/MS spectra of 4-CN Phe and 4-NO_2 Phe and that the combined loss of H_2O + CO is not observed in the CID MS/MS spectra of 4-NH_2 Phe. Thus the data points for these derivatives cannot be included in the respective construction of the Hammett plots.

Although the correlation coefficients for the competing pathways are rather poor, the data shown in Fig. 2 provide some useful insights.§ In Fig. 2a the sign of the reaction constant, ρ_{NH_3} (the slope of the Hammett plot), for the loss of NH_3 from substituted phenylalanine is negative. This is consistent with the above suggestion that the rate of NH_3 loss pathway is enhanced by an electron-donating substituent. In contrast, the Hammett plot for the competing loss of H_2O + CO has a positive reaction constant, ρ_{H_2O+CO}, suggesting that the rate of reaction is enhanced by an electron-withdrawing substituent (Fig. 1b). Additionally, the greater magnitude of the reaction constant for the NH_3 loss relative to the combined loss of H_2O + CO ($\rho_{H_2O+CO} < \rho_{NH_3}$) signifies that NH_3 loss pathway is more susceptible to a change in the substituent.

While the Hammett plots are suggestive of trends, they do not allow a distinction between the two competing pathways for NH_3 loss shown in Scheme 2, which would both benefit from electron-donating substituents. Shoeib *et al.* have proposed that a 1,2-hydride migration can compete with neighbouring group attack to form a benzyl cation structure **D** (pathway 3 in Scheme 2), and that the benzyl cation **D** is lower in energy than the phenonium ion **C** (Scheme 2) at the B3LYP/6-311++G(d,p) level of theory.[38] However, the transition state energy barrier for the 1,2-hydride migration pathway was estimated to be higher than the neighbouring group process to lose NH_3, which was proposed to be a barrierless process.[38] Note that related 1,2-hydride migration pathways have also been proposed as competing mechanisms for NH_3 loss from protonated serine[21] and cysteine[5,21] and in the solution-phase deamination of phenylalanine and derivatives.[26,27]

In order to gain further structural, energetic, and kinetic insights into these interesting substituent effects, in the next sections we have employed a combination of hybrid density functional theory (DFT) calculations at the B3LYP/6-31+G(d,p) level of theory with rate constant calculation using RRKM theory to: (a) evaluate whether the H_2O + CO loss pathway is insensitive to the substituent as suggested by the Hammett plot shown in Fig. 1b; (b) examine the two competitive NH_3 loss pathways shown in Scheme 2 for selected *para*-substituted phenylalanine derivatives; (c) estimate the transition state energy barriers for the competing fragmentation pathways (pathways 1, 2 and 3 in Scheme 2) of the same *para*-substituted phenylalanine derivatives and apply RRKM calculations to study how substituents influence the change in rate constant for the competing fragmentation pathways 1, 2, and 3.

(2) DFT and RRKM rate constant study of the combined loss of H_2O + CO from protonated *para*-substituted phenylalanine

The relative transition state energy barriers of competing fragmentation reactions are a useful guide to the observed relative product ion intensities from ion trap CID MS/MS due to the slow heating method of ion activation in the quadrupole ion trap mass spectrometer,[40] in which low energy fragmentation pathways are favoured. Thus we have used DFT calculations at the B3LYP/6-31+G(d,p) level of theory to examine the structures and energetics of the reactants, transition states and products for each of the competing fragmentation pathways (pathways 1, 2 and 3 in Scheme 2) for the protonated *para*-substituted phenylalanine derivatives (R = NH_2, OH, Me, H, Cl, NO_2).

Previous studies have shown that the combined loss of H_2O + CO is the most prevalent fragmentation pathway in protonated aliphatic amino acids.[21,22,41] Through H/D exchange studies and high level *ab initio* calculations, the combined loss of H_2O + CO is now generally accepted to proceed *via* a two step mechanism involving an initial intramolecular proton transfer from the ammonium group to hydroxyl OH, followed by the combined loss of H_2O and CO to form an immonium ion (structure **B** in Scheme 1).[41–43] Due to the high basicity of the amino group, the first intramolecular proton transfer step is generally accepted to be the rate determining step in the mechanism.¶ In order to address how the combined H_2O + CO loss pathway is influenced by ring substituents, we have examined the structures and energetics of selected protonated *para*-substituted phenylalanine derivatives (R_4 = NH_2, OH, Me, H, Cl, NO_2), ranging from electron-donating to electron-withdrawing.

The B3LYP/6-31+G(d,p) calculated potential energy surface (PES) for 4-NH_2 Phe, 4-OH Phe, Phe, and 4-NO_2 Phe are shown in Fig. 3. All related structures are shown in Fig. 4 for 4-NH_2 Phe and Fig. S4–8 in the supplementary material for 4-OH Phe, 4-Me Phe, Phe, 4-Cl Phe, and 4-NO_2 Phe, respectively. How these surfaces help explain the competition between NH_3 and H_2O + CO loss is discussed in further detail in Section 4. Here we focus on the details of the potential energy surface for combined H_2O + CO loss. This pathway is shown in red in the potential energy surfaces summary in Fig. 3 and Fig. S1 in the supplementary material. The dashed lines represent the rotational barrier interconnecting rotamers **A** and **A1**, which were not calculated. Examination of the potential energy surface for pathway 1 for all substituents studied computationally suggests that **TS1a** has the highest energy barrier for this pathway.

In all cases, the intramolecular proton transfer, **TS1a**, is a late transition state in which the H_2O molecule is already departing from the ion. This process has an estimated energy barrier of +39.2 kcal mol^{-1} for 4-NH_2 Phe, relative to the global minimum **A**. The product of the TS is an acylium–H_2O ion–molecule complex **I1a**, which is only more stable than **TS1a** by 0.1 kcal mol^{-1}. The subsequent transition state to lose carbon monoxide was found by slightly elongating the C–CO bond in the ion–molecule complex **I1a** to *ca.* 2.0 Å, and then optimizing for a transition state. The resultant transition state, **TS1b**, is slightly lower in energy than the ion–molecule complex **I1a** for all substituents calculated, suggestive that the subsequent loss of CO is instantaneous after the first intramolecular proton transfer step (shown in Fig. 4 for 4-NH_2 Phe and supplementary Fig. S4–8 for other substituents calculated). This phenomenon has previously been observed in a computational study of the fragmentation of protonated glycine,[41] and is consistent with our experimental result that the sole loss of H_2O is not observed

§ A reviewer has correctly pointed out that Hammett linear free-energy correlations are generally used to address the influence of substituents on either equilibrium constants or absolute rate constants. Unfortunately the determination of absolute gas phase unimolecular dissociation rate constants is largely limited to the blackbody infrared dissociation (BIRD) technique,[49] which requires specialized instrumentation.

¶ There is another plausible mechanism for the loss of H_2O + CO. It involves an initial intramolecular proton transfer from amino group to C1 of phenyl ring, followed by another intramolecular proton transfer to the hydroxyl oxygen, and then the subsequent simultaneous loss of H_2O + CO to form the same immonium ion. However, it was found that this mechanism cannot compete with the generally accepted mechanism, even when an electron-donating group (4-NH_2) is present in the phenyl ring (data not shown). Therefore, the transition state barriers for the loss of H_2O + CO from other phenylalanine derivatives *via* this mechanism were not calculated.

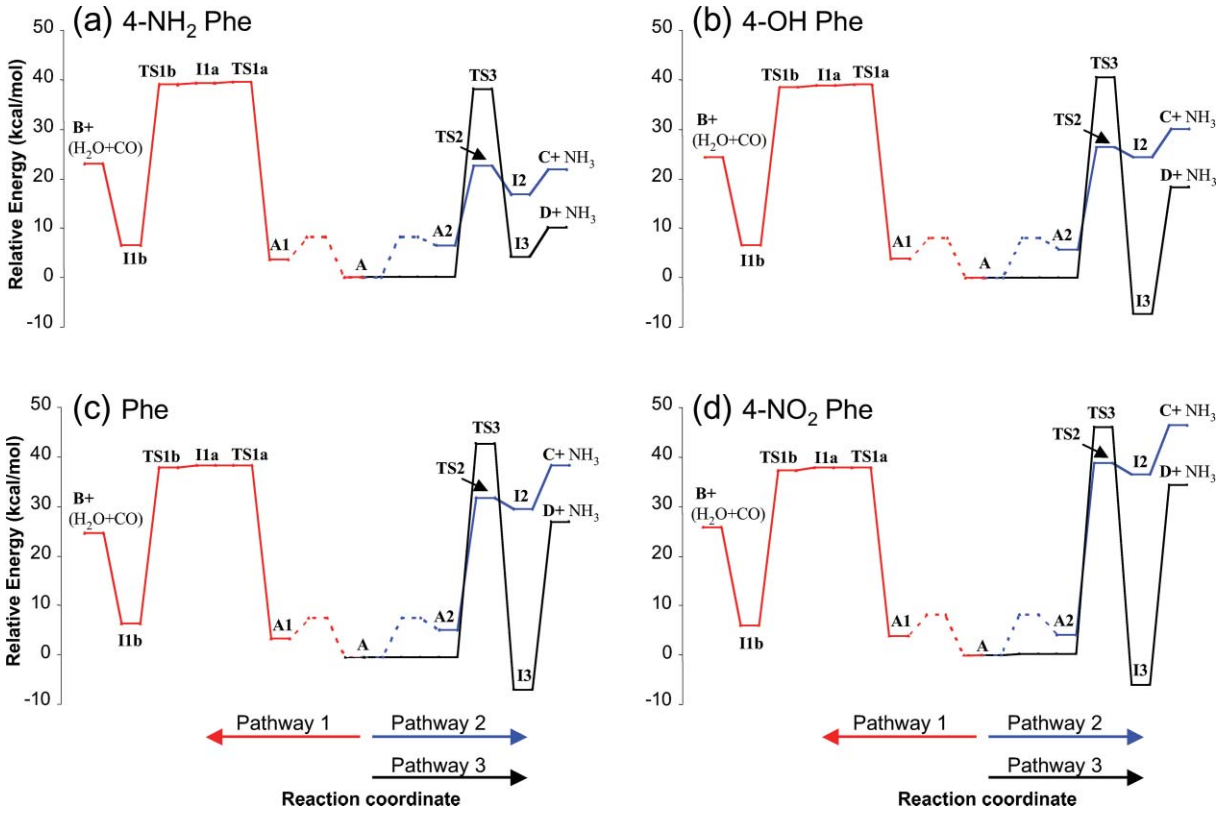

Fig. 3 The B3LYP/6-31+G(d,p) calculated potential energy surfaces for the competing fragmentation pathways 1–3 shown in Scheme 2 for protonated (a) 4-NH_2 Phe, (b) 4-OH Phe, (c) Phe, and (d) 4-NO_2 Phe. All energies are relative to global minimum **A**. The combined H_2O + CO loss (pathway 1 in Scheme 2) is represented by the red PES, NH_3 loss by neighbouring group mechanism (pathway 2 in Scheme 2) is represented by the blue PES, and NH_3 loss by 1,2-hydride migration process (pathway 3 in Scheme 2) is represented by the black PES. Dashed lines represent transition states (which were not located) interconnecting conformers.

(Fig. 2). The combined energy of the separated products (the immonium ion **B** and H_2O + CO) yields a relative energy of +22.9 kcal mol^{-1} for protonated 4-NH_2 Phe. Our DFT calculations at B3LYP/6-31+G(d,p) level of theory thus confirm that the first intramolecular proton transfer step is the rate determining step (Fig. 3 and Fig. S4–8).

How is the barrier for H_2O + CO loss influenced by the substituent? An examination of Table 2, which lists the calculated relative transition state energy barriers and the relative energy of the separated products (structure **B**, **C**, and **D**) with H_2O + CO for the selected series of *para*-substituted phenylalanine derivatives, shows a clear decrease in the transition state energy as the substituent becomes more electron-withdrawing. The net change from the most electron-donating to the most electron-withdrawing substituent is, however, small, suggesting that the reaction is largely unaffected by the nature of the substituent. Not only is this result consistent with the smaller magnitude in the reaction constant (ρ_{H_2O+CO}) for combined H_2O + CO loss (Fig. 2b) compared to that for NH_3 loss (Fig. 2a), but it is also consistent with the relative rate constants predicted using RRKM modelling. These RRKM calculations, which utilize the transition state energy barrier of **TS1a** and vibrational frequencies of the global minimum and appropriate transition state from DFT calculations, clearly show that the rates are insensitive to the substituent (see supplementary Fig. S3a).

(3) DFT and RRKM rate constant study of the NH_3 loss from protonated substituted phenylalanine

The B3LYP/6-31+G(d,p) calculated potential energy surface and optimized structures for the reaction profile for the loss of NH_3 for 4-NH_2 Phe (pathways 2 and 3 in Scheme 2) are shown in Fig. 3a and Fig. 4, respectively. The neighbouring group pathway for NH_3 loss (pathway 2 in Scheme 2) is represented by the blue potential energy surface, while the potential energy surface for the competing 1,2-hydride migration pathway (pathway 3 in Scheme 2) is shown in black (Fig. 3 and S1). In the neighbouring group pathway (pathway 2 of Scheme 2) the loss of NH_3 occurs by intramolecular nucleophilic attack by the C1 atom of the aromatic side chain *via* structure **TS2** to form the phenonium ion **C**. The estimated transition state energy of **TS2** is +22.4 kcal mol^{-1}, relative to the global minimum of 4-NH_2 Phe (structure **A**), while the relative energy of the separated product **C** +NH_3 is comparable at +21.6 kcal mol^{-1}. Interestingly, the **TS2** energy of +22.4 kcal mol^{-1} is comparable to the transition state energy barrier for NH_3 loss from protonated tryptophan, which fragments *via* a similar neighbouring group mechanism.[7] For the competing 1,2-hydride migration pathway (pathway 3 of Scheme 2), the transition state adopts a planar structure (structure **TS3**), and the hydride ion migrates from β- to α-position in an anti-position relative to the departing NH_3 leaving group.‖ Although the product benzyl cation **D** has a resulting positive charge on the β-position, which can be resonance stabilized by the aromatic ring, this process has a calculated relative transition state energy barrier of +37.9 kcal mol^{-1}.

In order to address how the competition between these two NH_3 loss pathways is influenced by other ring substituents, we have examined the structures and energetics of other protonated *para*-substituted phenylalanine derivatives (R_4 = OH, Me, H, Cl, NO_2), ranging from electron-donating to electron-withdrawing (see data from Fig. S4–8 in the supplementary material). The key relative transition state energies and the overall reaction energetics are also summarized in Table 2. It is important to note that the endothermicities of the neighbouring group pathway are greater than the transition state barrier for all substituents

‖A reviewer has pointed out that the transition state **TS3** is in fact a dyotropic rearrangement involving H and NH_3. However, the subsequent loss of NH_3 to produce the benzyl cation **D** *via* C–NH_3 bond stretching is expected to be barrierless.

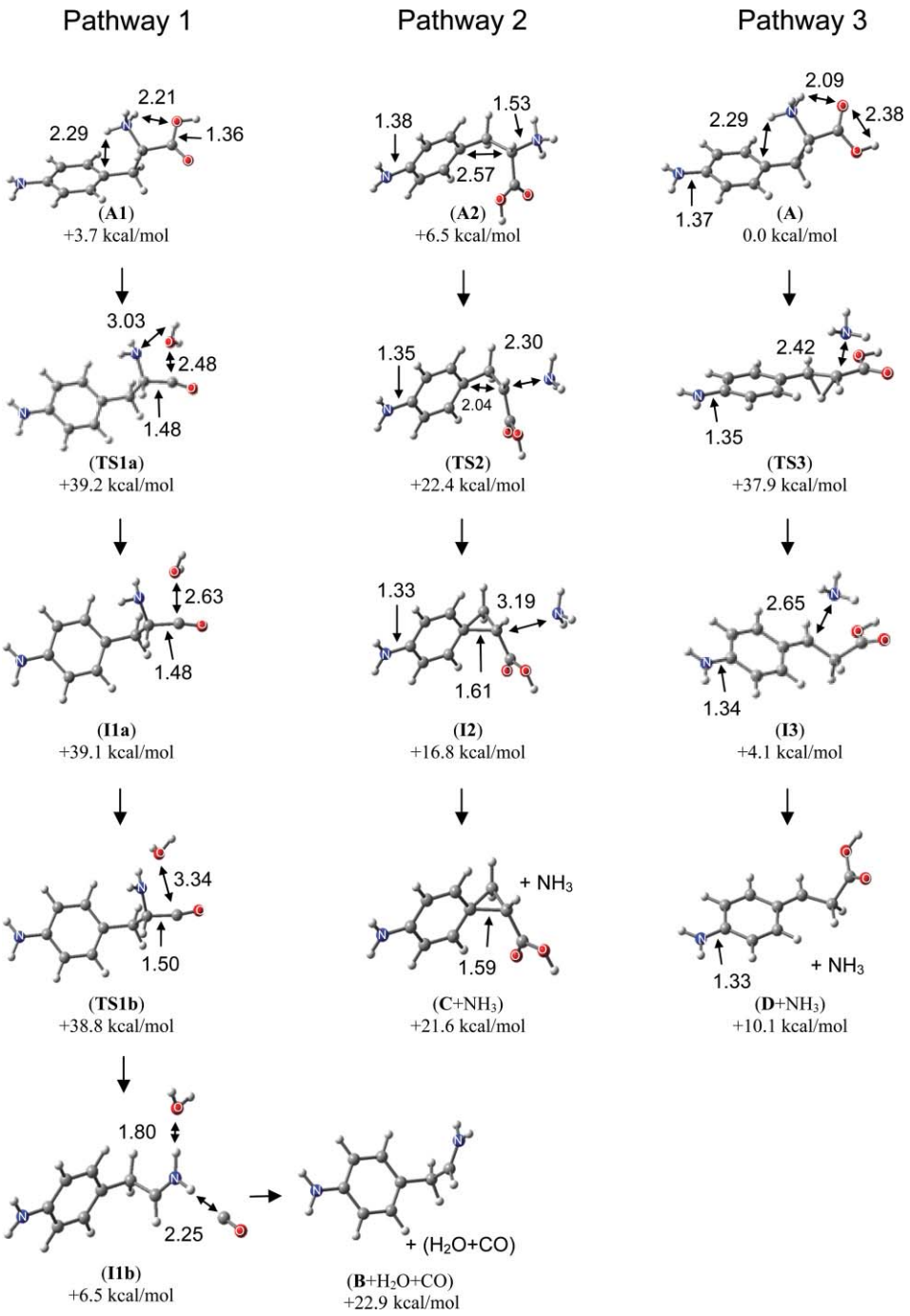

Fig. 4 B3LYP/6-31+G(d,p) optimized structures and relative energies for all species in the competing pathways 1–3 in Scheme 2 for protonated 4-NH_2 Phe. All energy values are relative to the global minimum **A**.

studied computationally, except for 4-NH_2 Phe. An examination of Table 2 also shows that NH_3 loss *via* the neighbouring group process is the kinetically favoured product as the transition state energy barriers (and the reaction endothermicities) are lower than the transition state barrier for the hydride migration process in nearly all cases. The exception is 4-NO_2 Phe, which has a transition state barrier for the competing 1,2-hydride migration process which is comparable in energy to the reaction endothermicity for NH_3 loss by the neighbouring group pathway. In contrast, the overall reaction energetics show that the hydride migration process is the thermodynamically favoured product, which is not surprising since this pathway yields the stabilised benzyl cation. Thus, the competition between the two pathways for NH_3 loss highlights that gas phase fragmentation reactions are under kinetic control rather than thermodynamic control (pathway 2 of Scheme 2 would be preferred).

Both the neighbouring group and hydride migration processes for NH_3 loss show an increase in transition state energy as the substituent becomes more electron-withdrawing, consistent with the negative reaction constant (ρ_{NH_3}) of the Hammett plot (Fig. 2a). This increase in transition state energy barriers for both neighbouring group and hydride migration process is expected since, in the former pathway, the side chain loses the neighbouring group ability as the substituent becomes more electron-withdrawing. Similarly, in the hydride migration pathway, the substituent lacks the ability to resonance-stabilize the benzyl cation when the substituent becomes more electron-withdrawing. Table 2 also shows that the increase in the transition state energy barrier is greater for the neighbouring group process, indicating that the neighbouring group process is more susceptible to a change in the substituent. This is borne out by the RRKM calculations, which show a larger spread in rates

Table 2 Calculated transition energy barrier (at B3LYP/6-31+G(d,p)) and the relative energy of the separated products (ΔE_R) for the competing fragmentation processes for 4-NH_2 Phe, 4-OH Phe, 4-Me Phe, Phe, 4-Cl Phe, and 4-NO_2 Phe. All energy values are relative to the global minimum **A**

	TS energy, $\Delta E^{\ddagger}$/kcal mol^{-1}			ΔE_R/kcal mol^{-1}		
Phenylalanine derivative[a]	Pathway 1[b] (H_2O + CO loss)	Pathway 2[c] (NH_3 loss by neighbouring group)	Pathway 3[d] (NH_3 loss by 1,2-hydride migration)	Pathway 1[b] (H_2O + CO loss)	Pathway 2[c] (NH_3 loss by neighbouring group)	Pathway 3[d] (NH_3 loss by 1,2-hydride migration)
$R_4 = NH_2$[e]	39.2	22.4	37.9	22.9	21.6	10.1
$R_4 = OH$[f]	39.1	26.5	40.8	24.4	30.1	18.4
$R_4 = Me$[g]	39.3	29.0	42.2	24.9	34.4	22.9
$R_4 = H$[h]	39.1	32.5	43.6	25.3	39.1	27.6
$R_4 = Cl$[i]	38.7	37.1	43.1	25.1	37.2	25.3
$R_4 = NO_2$[j]	37.8	38.7	45.9	25.8	46.4	34.3

[a] Listed according to increasing electron-withdrawing capability (more positive σ^+). See Scheme 1 for structures. [b] Yield of the immonium ion **B** is shown in Scheme 2. The TS energy listed is the rate limiting step involving intramolecular proton transfer from ammonium to hydroxyl group. The PES for the reaction is shown in red in Fig. 3 and supplementary Fig. S1. [c] NH_3 loss *via* neighbouring group pathway is shown in Scheme 2. The PES for the reaction is shown in blue in Fig. 3 and supplementary Fig. S1. [d] NH_3 loss *via* 1,2-hydride migration pathway is shown in Scheme 2. The PES for the reaction is shown in black in Fig. 3 and supplementary Fig. S1. [e] Full PES is shown in Fig. 3a. [f] Full PES is shown in Fig. 3b. [g] Full PES is shown in supplementary Fig. S1a. [h] Full PES is shown in Fig. 3c. [i] Full PES is shown in supplementary Fig. S1b. [j] Full PES is shown in Fig. 3d.

for the neighbouring group pathway than for the 1,2-hydride pathway (compare supplementary Fig. S3b and S3c).

(4) Rationalizing the relative abundances for the competing pathways using both the DFT and RRKM data

Utilizing all of the theoretical data (Table 2, Fig. 3, 5 and supplementary Fig. S1–3), it is now possible to get a more complete picture of the change in reaction products as a function of the substituent on the ring. The RRKM kinetics correctly predict that NH_3 loss should dominate for the strongly electron-donating substituents (NH_2 and OH, Fig. 5a–b) and also show that while the H_2O +CO pathway (**TS1a**) is insensitive to the nature of the substituent (supplementary Fig. S3a), the NH_3 losses are significantly affected by the substituent (supplementary Fig. S3b–c). It is clear, however, that it is not sufficient to only consider the transition state barriers and the resultant RRKM kinetics. For example, the rates for NH_3 loss *via* the neighbouring group pathway and the H_2O +CO pathway are virtually identical for 4-NO_2 Phe (Fig. 5d) and yet H_2O + CO loss dominates the mass spectrum (Fig. 1d). Thus the RRKM data needs to be used in conjunction with the full PES, particularly the final reaction energetics (*i.e.*, for the separated products). For the strongly electron-donating substituents (R_4= NH_2 and OH, Fig. 5a–b), both the transition state barrier (**TS2**) and the overall reaction energetics lie below that of the transition state barrier for the H_2O +CO pathway (**TS1a**) and thus NH_3 loss predominates. As the ring become less nucleophilic both the transition state barrier (**TS2**) and the overall reaction energetics for the neighbouring group loss of NH_3 significantly increase in energy, while the transition state barrier for the H_2O + CO pathway (**TS1a**) remains virtually unchanged. Moreover, in all cases, the final energetics for the H_2O + CO pathway is lower than **TS1a** and thus the H_2O + CO pathway becomes more significant for electron-withdrawing substituents. Thus, the reason that H_2O + CO loss dominates for 4-NO_2 is the energy for separated reactants (**C** + NH_3) is now larger than **TS1a** (Fig. 3d) by 8.6 kcal mol^{-1}.

(5) Comparisons with previous condensed phase and gas phase studies

Numerous studies have examined the formation and reactions of phenonium ions related to **C** in both the condensed and gas phases.[44,45] Of particular relevance to the competition between NH_3 loss *via* the aryl neighbouring group pathway (pathway 2 of Scheme 2) and the hydride pathway (pathway 3 of Scheme 2) are the gas phase studies of Speranza on the stereochemical outcomes of acid-induced dissociation of optically active phenylpropanols (Scheme 3)[46,47] and the condensed-phase nitrous acid induced deamination of *para*-substituted phenylalanine derivatives (substituent, R = OMe, H, NO_2) (Scheme 4).[26,27]

Speranza has examined the acid-induced dissociation of optically active phenylpropanols in the gas phase *via* an analysis of kinetic and stereochemical outcomes[46] as well as deuterium isotope effects.[47] Both studies point to a unified picture, as illustrated for (*S*)-2-phenyl-1-propanol in Scheme 3. It is noteworthy that the loss of the leaving group occurs *via* three pathways: (i) hydride migration yields the substituted benzyl cation **E**; (ii) methide migration yields the substituted benzyl cation **F**; (iii) participation by the phenyl group yields the intermediate **G**. All the observed products can be rationalized as arising from each of these three intermediates. Thus, there are clear analogies between pathways 2 and 3 of Scheme 2 for the loss of NH_3 from phenylalanine and its derivatives.

Condensed phase nitrous acid induced deamination of *para*-substituted phenylalanine derivatives (substituent, R_4 = OMe, H, NO_2) also leads to a complex series of products (**H1**–**H5** of Scheme 4).[26,27] When trifluoroacetic acid (TFA) is used as the solvent, the majority of the deamination products of *para*-substituted phenylalanine derivatives are formed by phenyl

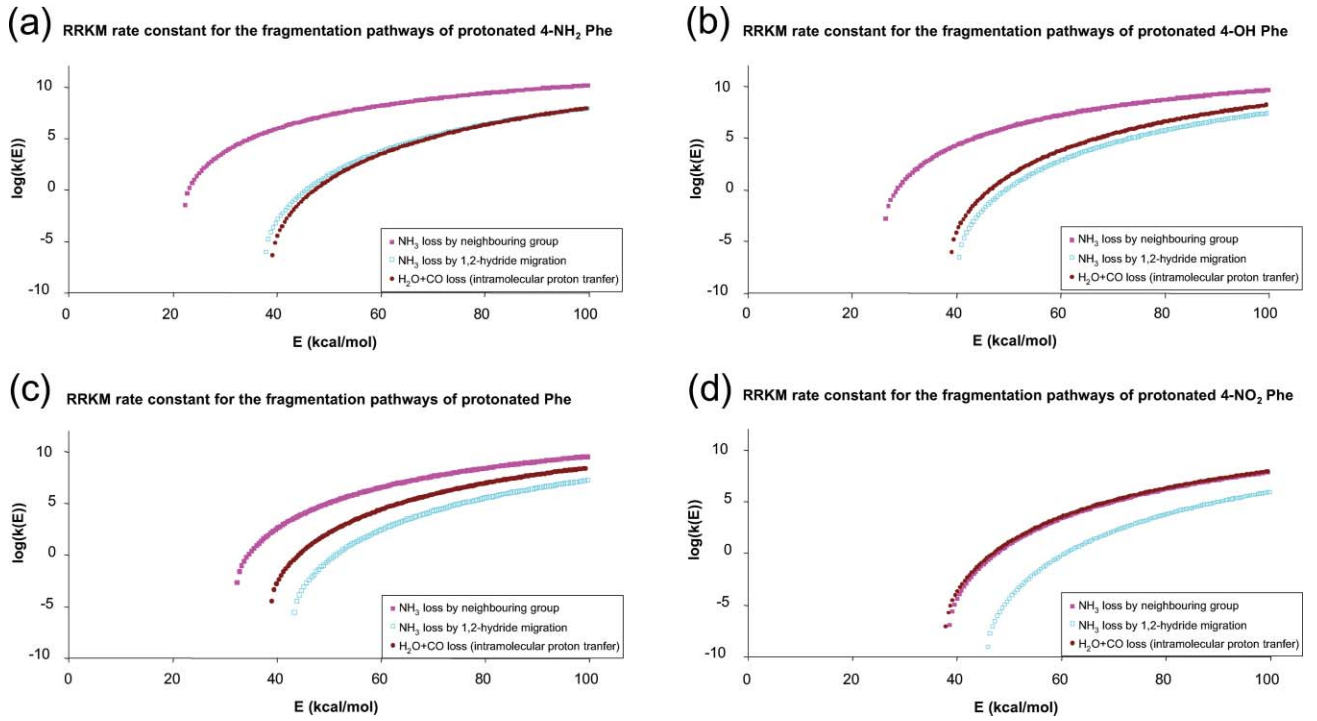

Fig. 5 RRKM unimolecular rate constant for the competitive fragmentation reactions 1–3 shown in Scheme 2 for protonated (a) 4-NH_2 Phe, (b) 4-OH Phe, (c) Phe, and (d) 4-NO_2 Phe.

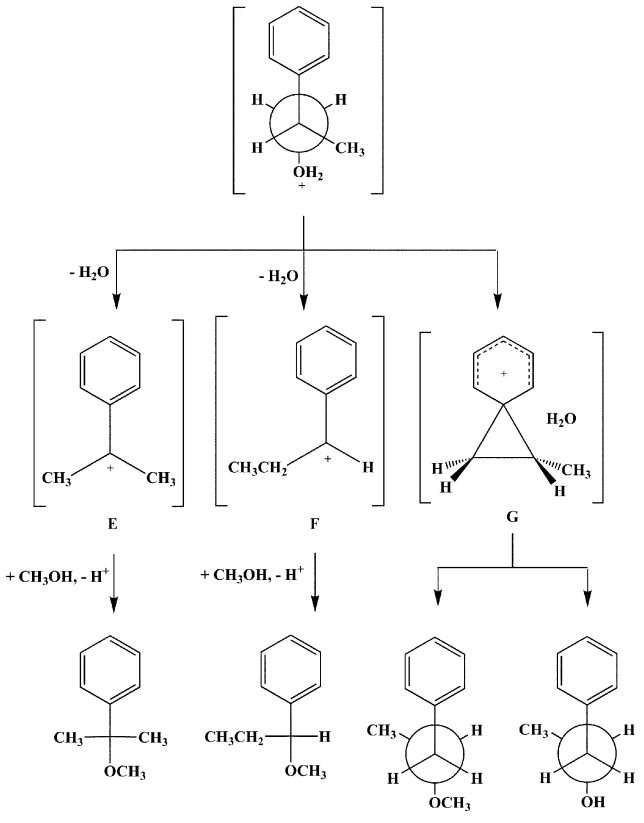

Scheme 3

migration mechanism if the substituent is electron-donating (see Scheme 4 for their relative yields in TFA).[26,27] However, when the reaction was performed using acetic or sulfuric acid, other products arising from hydrogen migration, elimination, and substitution were also observed. Hence, the phenyl migration pathway appears to have the lowest energy barrier under the conditions of low nucleophilicity and high ionizing power of TFA.[26,27] Indeed, there is an interesting correlation between our gas phase results and these condensed phase solvolysis reactions for the same substituents (R_4 = OMe, H, and NO_2). Thus, for the most electron-donating substituent (R_4 = OMe) the phenyl neighbouring group pathway dominates both in the gas phase (Tables 1 and 2) as well as in the condensed phase (Scheme 4). In contrast, when $R_4 = NO_2$ (an electron-withdrawing group) this pathway is suppressed in both the gas and condensed phase.

Conclusions

The combined use of collisional activation in a quadrupole ion trap mass spectrometer, application of the Hammett equation and molecular orbital calculations coupled with RRKM theory have proven to be a powerful combination to examine the gas-phase reactions of protonated phenylalanine and its *para*-substituted derivatives. Protonated phenylalanine and derivatives with electron-withdrawing substituents favour the loss of H_2O + CO. In contrast, electron-donating substituents promote the loss of NH_3. DFT calculations on a range of phenylalanine derivatives reveal that in most cases three competing mechanisms can potentially occur: H_2O + CO loss (pathway 1 of Scheme 2); NH_3 loss *via* an aryl neighbouring group reaction (pathway 2 of Scheme 2); and NH_3 loss *via* a 1,2 hydride migration reaction (pathway 3 of Scheme 2). The activation barriers and the resultant RRKM kinetics are predicted to vary for each of these processes, depending on the nature of the substituent. For the electron-donating substituents (4-NH_2, 4-OH and 4-Me), the barriers are in the order: pathway 2 < pathway 1 < pathway 3. In order to rationalize the experimentally observed reaction yields for competing H_2O + CO loss and NH_3 loss, however, the RRKM data needs to be used in conjunction with the full PES, particularly the final reaction energetics. In addition, there are interesting correlations between our gas phase data and condensed phase solvolysis reactions of related phenylalanine derivatives.

An ultimate goal in the field of analytical mass spectrometry is to control the gas phase fragmentation of biomolecules. In the area of amino acid and peptide analysis, it may be possible to exert such a control through the rational design of appropriate derivatives which change the nature of either

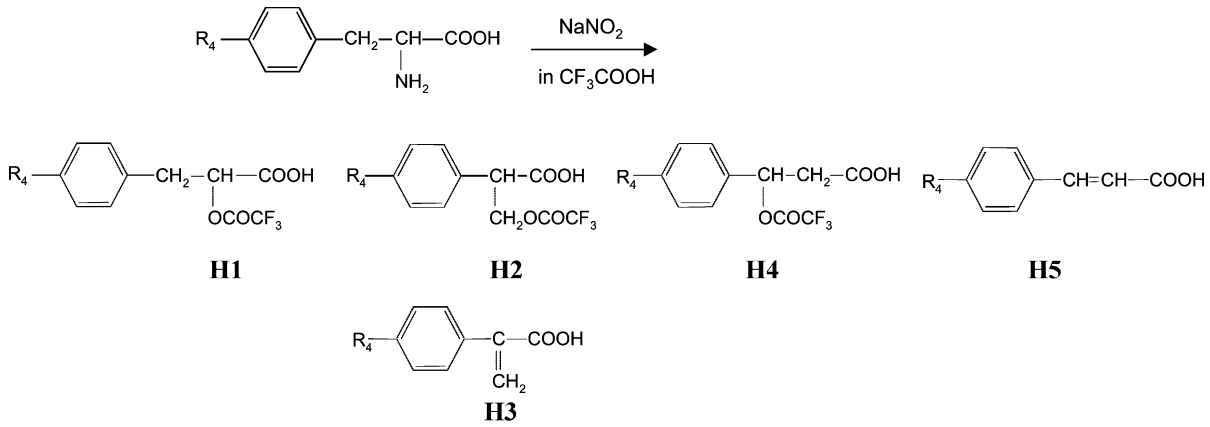

H1 **H2** **H4** **H5**

H3

Starting material	Yield of Deamination Products (% yield) [a]			
	Substitution products **H1**	Phenyl migration products **H2** and **H3**	Hydrogen migration products **H4**	Elimination products **H5**
$R_4 = OCH_3$	5	93	0	0
$R_4 = H$	25	63	10	2
$R_4 = NO_2$	72	0	0	0

[a] Results were adapted from reference 27

Scheme 4

the electrophile or nucleophile in neighbouring group reactions. This work demonstrates that enhancing the nucleophilicity of the neighbouring group nucleophile promotes NH_3 loss. We have also recently demonstrated that the use of fixed charge derivatives in peptides can isolate the electrophile at a specific site (*e.g.*, methionine residues) and thereby provide structurally diagnostic information.[48]

Acknowledgements

The authors would like to thank Associate Professor Jonathan M. White for helpful discussions on various aspects of the Hammett plot. Dr Julia Laskin is gratefully acknowledged for useful discussion on RRKM theory. R.A.J.O. thanks the Australian Research Council (ARC) for financial support. H.L. acknowledges the award of an Elizabeth and Vernon Puzey Postgraduate Research Scholarship. Support of the Victorian Institute for Chemical Sciences High Performance Computing Facility is gratefully acknowledged.

References

1 R. Aebersold and D. R. Goodlett, *Chem. Rev.*, 2001, **101**, 269–296.
2 R. A. J. O'Hair, *J. Mass Spectrom.*, 2000, **35**, 1377–1381.
3 E. A. Kapp, F. Schuetz, G. E. Reid, J. S. Eddes, R. L. Moritz, R. A. J. O'Hair, T. P. Speed and R. J. Simpson, *Anal. Chem.*, 2003, **75**, 6251–6264.
4 B. Capon and S. P. McManus, *Neighboring Group Participation, Vol. 1*, Plenum Press, 1976.
5 R. A. J. O'Hair, M. L. Styles and G. E. Reid, *J. Am. Soc. Mass Spectrom.*, 1998, **9**, 1275–1284.
6 C. D. Maycock and R. J. Stoodley, *J. Chem. Soc., Perkin Trans. 1*, 1979, 1852–1857.
7 H. Lioe, R. A. J. O'Hair and G. E. Reid, *J. Am. Soc. Mass Spectrom.*, 2004, **15**, 65–76.
8 J. E. Johansen, B. D. Christie and H. Rapoport, *J. Org. Chem.*, 1981, **46**, 4914–4920.
9 B. Paizs and S. Suhai, *Mass Spectrom. Rev.*, 2005, **24**, 508–548.
10 F. W. McLafferty, *Anal. Chem.*, 1959, **31**, 477.
11 M. M. Bursey and F. W. McLafferty, *J. Am. Chem. Soc.*, 1966, **88**, 529–536.
12 M. M. Bursey and F. W. McLafferty, *J. Am. Chem. Soc.*, 1966, **88**, 4484–4488.
13 M. M. Bursey and F. W. McLafferty, *J. Am. Chem. Soc.*, 1967, **89**, 1–6.
14 M. S. Chin and A. G. Harrison, *Org. Mass Spectrom.*, 1969, **2**, 1073–1083.
15 M. M. Bursey, in *Advances in Linear Free Energy Relationships*, ed. N. B. Chapman and J. Shorter, Plenum Press, New York, 1972, ch. 10, pp. 445–461.
16 A. G. Harrison, *J. Mass Spectrom.*, 1999, **34**, 577–589.
17 D. G. Morgan and M. M. Bursey, *Org. Mass Spectrom.*, 1994, **29**, 354–359.
18 D. G. Morgan and M. M. Bursey, *J. Mass Spectrom.*, 1995, **30**, 290–295.
19 A. G. Harrison, *Int. J. Mass Spectrom.*, 2002, **217**, 185–193.
20 A. G. Harrison, I. G. Csizmadia, T.-H. Tang and Y.-P. Tu, *J. Mass Spectrom.*, 2000, **35**, 683–688.
21 F. Rogalewicz, Y. Hoppilliard and G. Ohanessian, *Int. J. Mass Spectrom.*, 2000, **195/196**, 565–590.
22 N. N. Dookeran, T. Yalcin and A. G. Harrison, *J. Mass Spectrom.*, 1996, **31**, 500–508.
23 H. El Aribi, G. Orlova, A. C. Hopkinson and K. W. M. Siu, *J. Phys. Chem. A*, 2004, **108**, 3844–3853.
24 W. Kulik and W. Heerma, *Biomed. Environ. Mass Spectrom.*, 1988, **15**, 419–427.
25 G. W. Milne, T. Axenrod and H. M. Fales, *J. Am. Chem. Soc.*, 1970, **92**, 5170–5175.
26 K. Koga, C. C. Wu and S. Yamada, *Chem. Pharm. Bull.*, 1972, **20**, 1272–1281.
27 K. Koga, C. C. Wu and S. Yamada, *Chem. Pharm. Bull.*, 1972, **20**, 1282–1286.
28 H. C. Brown and Y. Okamoto, *J. Am. Chem. Soc.*, 1958, **80**, 4979–4987.
29 C. Hansch, A. Leo and R. W. Taft, *Chem. Rev.*, 1991, **91**, 165–195.
30 G. W. Trucks, H. B. Schlegel, G. E. Scuseria, M. A. Robb, J. R. Cheeseman, J. A. Montgomery, Jr., T. Vreven, K. N. Kudin, J. C. Burant, J. M. Millam, S. S. Iyengar, J. Tomasi, V. Barone, B. Mennucci, M. Cossi, G. Scalmani, N. Rega, G. A. Petersson, H. Nakatsuji, M. Hada, M. Ehara, K. Toyota, R. Fukuda, J. Hasegawa, M. Ishida, T. Nakajima, Y. Honda, O. Kitao, H. Nakai, M. Klene, X. Li, J. E. Knox, H. P. Hratchian, J. B. Cross, C. Adamo, J. Jaramillo, R. Gomperts, R. E. Stratmann, O. Yazyev, A. J. Austin, R. Cammi, C. Pomelli, J. W. Ochterski, P. Y. Ayala, K. Morokuma, G. A. Voth, P. Salvador, J. J. Dannenberg, V. G. Zakrzewski, S. Dapprich, A. D. Daniels, M. C. Strain, O. Farkas, D. K. Malick, A. D. Rabuck,

K. Raghavachari, J. B. Foresman, J. V. Ortiz, Q. Cui, A. G. Baboul, S. Clifford, J. Cioslowski, B. B. Stefanov, G. Liu, A. Liashenko, P. Piskorz, I. Komaromi, R. L. Martin, D. J. Fox, T. Keith, M. A. Al-Laham, C. Y. Peng, A. Nanayakkara, M. Challacombe, P. M. W. Gill, B. Johnson, W. Chen, M. W. Wong, C. Gonzalez, and J. A. Pople, *GAUSSIAN 03 (Revision B.04)*, Gaussian, Inc., Pittsburgh PA, 2003.
31 W. J. Hehre, J. A. Pople, and L. Radom, Ab Initio *Molecular Orbital Theory*, Wiley Interscience, 1986, pp. 78–82.
32 G. Z. Whitten and B. S. Rabinovitch, *J. Chem. Phys.*, 1963, **38**, 2466–2473.
33 T. Baer and P. M. Mayer, *J. Am. Soc. Mass Spectrom.*, 1997, **8**, 103–115.
34 K. A. Holbrook, M. J. Pilling, and S. H. Robertson, *Unimolecular Reactions, 2nd Edn*, John Wiley and Sons, 1996, ch. 4, pp. 94–99.
35 J. Laskin and J. H. Futrell, *Mass Spectrom. Rev.*, 2003, **22**, 158–181.
36 J. Laskin, *Eur. J. Mass Spectrom.*, 2004, **10**, 259–267.
37 J. Laskin and J. H. Futrell, *Mass Spectrom. Rev.*, 2005, **24**, 135–167.
38 T. Shoeib, A. Cunje, A. C. Hopkinson and K. W. M. Siu, *J. Am. Soc. Mass Spectrom.*, 2002, **13**, 408–416.
39 H. Kang, C. Jouvet, C. Dedonder-Lardeux, S. Martrenchard, G. Gregoire, C. Desfrancois, J. P. Schermann, M. Barat and J. A. Fayeton, *Phys. Chem. Chem. Phys.*, 2005, **7**, 394–398.
40 S. A. McLuckey and D. E. Goeringer, *J. Mass Spectrom.*, 1997, **32**, 461–474.
41 R. A. J. O'Hair, P. S. Broughton, M. L. Styles, B. T. Frink and C. M. Hadad, *J. Am. Soc. Mass Spectrom.*, 2000, **11**, 687–696.
42 F. Rogalewicz and Y. Hoppilliard, *Int. J. Mass Spectrom.*, 2000, **199**, 235–252.
43 B. Balta, M. Basma, V. Aviyente, Z. Chuanbao and C. Lifshitz, *Int. J. Mass Spectrom.*, 2000, **201**, 69–85.
44 C. J. Lancelot, D. J. Cram and P. v. R. Schleyer, *Carbonium Ions*, 1972, **3**, 1347–1483.
45 E. del Rio, M. I. Menendez, R. Lopez and T. L. Sordo, *J. Am. Chem. Soc.*, 2001, **123**, 5064–5068.
46 M. Speranza and A. Filippi, *Chem. Eur. J.*, 1999, **5**, 834–844.
47 M. Speranza and A. Filippi, *Chem. Eur. J.*, 1999, **5**, 845–853.
48 G. E. Reid, K. D. Roberts, R. J. Simpson and R. A. J. O'Hair, *J. Am. Soc. Mass Spectrom.*, 2005, **16**, 1131–1150.
49 R. C. Dunbar, *Mass Spectrom. Rev.*, 2004, **23**, 127–158.
50 Part 44: C. K. Barlow, W. D. McFadyen and R. A. J. O'Hair, *J. Am. Chem. Soc.*, 2005, **127**, 6109–6115.